Biophysical Journal Volume 102 June 2012 2481–2488

What Is the Core Oscillator in the Speract-Activated Pathway of the *Strongylocentrotus purpuratus* Sperm Flagellum?

Luis U. Aguilera, Blanca E. Galindo, Daniel Sánchez, and Moisés Santillán*
Centro de Investigación y de Estudios Avanzados del Instituto Politécnico Nacional, Unidad Monterrey, Parque de Investigación e Innovación Tecnológica, Apodaca, México

ABSTRACT Sperm chemotaxis has an important role in fertilization. Most of our knowledge regarding this phenomenon comes from studies in organisms whose fertilization occurs externally, like sea urchins. Sea urchin spermatozoa respond to sperm-activating peptides, which diffuse from the egg jelly coat and interact with their receptor in the flagellum, triggering several physiological responses: changes in membrane potential, intracellular pH, cyclic nucleotide levels, and intracellular Ca^{2+} concentration ($[Ca^{2+}]$). In particular, flagellar $[Ca^{2+}]$ has been shown to oscillate. These $[Ca^{2+}]$ oscillations are correlated with changes in the flagellar shape and so with the regulation of the sperm swimming paths. In this study, we demonstrate, from a mathematical modeling perspective, that the reported speract-activated signaling pathway in *Strongylocentrotus purpuratus* (speract being a sperm-activating peptide specific to this species) has the necessary elements to replicate the reported $[Ca^{2+}]$ oscillations. We further investigate which elements of this signaling pathway constitute the core oscillator.

INTRODUCTION

The detection of chemical clues in the environment—which provide information on food, mates, toxics, predators, and pathogens—is essential for the survival of most leaving beings (1). Intracellular biochemical signaling mediated by ion channels is involved in sensory responses in diverse cell types, ranging from neurons to sperm (2).

In organisms of external fertilization, such as the sea urchin, both eggs and sperm are released to the environment. Due to the enormous dilution volume, which decreases the probability for the sperm to encounter the egg, these organisms have developed different strategies to fulfill fertilization. Some of them are: a large gamete production, an increased apparent egg size, and production of diffusible chemoattractants (3). Sea urchin sperm motility is modulated and guided toward the egg by a gradient of small peptides that diffuse from the egg jelly coat, carrying the signals to guide the sperm by a chemotaxis process. Chemotaxis requires the sperm to be able to accurately detect the chemoattractant concentration and respond by modifying its flagellar movement, resulting in a regulation of its swimming path (4).

Two different sea urchin species have been extensively studied: *Strongylocentrotus purpuratus* and *Arbacia punctulata* (5,6). Only in the last species has chemotaxis been fully proved. In this case, chemotaxis is mediated by resact, a tetradecapeptide produced in the egg jelly coat (7). In *S. purpuratus*, the decapeptide speract, a sperm-activating peptide (SAP) largely studied and analog to resact, induces sperm changes in ionic fluxes, second messenger concentrations, and membrane potential, similar to those produced by resact (5).

In *S. purpuratus,* speract has been demonstrated to bring about complex spatio-temporal patterns in the intracellular concentration of Ca^{2+} ($[Ca^{2+}]$). A precise control of the Ca^{2+} flux is necessary to achieve this complex Ca^{2+} signaling, which in turn induces modifications in the flagellar beat: when $[Ca^{2+}]$ is low, the flagella beat symmetrically, whereas in high $[Ca^{2+}]$ conditions, the flagellar beat becomes asymmetrical (8).

The $[Ca^{2+}]$ kinetics in response to speract is different in the sperm head and flagellum. In the head, the $[Ca^{2+}]$ increase is a tonic event, whereas in the flagellum, single cell measurements have revealed an oscillatory behavior (9–12). It has been demonstrated that the number of $[Ca^{2+}]$ oscillations depends on the SAP concentration used to stimulate the sperm (11). Additionally, the $[Ca^{2+}]$ increase propagates from the sperm flagellum to the head. Hence, the information of where the ligand is bound is lost, making this a temporal detection mechanism rather than a spatial one (9).

Despite great advances in the last few years, the *S. purpuratus* complete SAP-activated signaling pathway remains to be fully elucidated (5,6). The proposed underlying molecular mechanisms are as follows: speract binds to its receptor on the sperm flagellum; this interaction physically activates a membrane guanylyl cyclase, producing a rapid and transient cGMP increment (13,14); this in turn induces a K^+ efflux by direct activation of potassium-selective and cyclic nucleotide-gated channels (KCNG), making the sperm membrane potential more negative (15); this hyperpolarization activates a potassium-dependent sodium/calcium exchanger (NCKX), as well as a sodium-proton exchanger and a hyperpolarization-activated and cyclic nucleotide-gated sodium channel (HCN); all this results in intracellular alkalinization that induce a Na^+ influx and activates a soluble adenylyl cyclase, with the resulting

Submitted November 4, 2011, and accepted for publication March 29, 2012.
*Correspondence: msantillan@cinvestav.mx
Editor: Richard Bertram.

0006-3495/12/06/2481/8 $2.00
doi: 10.1016/j.bpj.2012.03.075

increase in cAMP (5); the hyperpolarization further removes the inactivation of voltage-dependent Ca^{2+} channels—given the membrane potential at which the Ca^{2+} influx starts, these channels are more likely low voltage-activated Ca^{2+}-channels; the resulting Ca^{2+} influx contributes to the sperm membrane depolarization (15); it has been proposed that high voltage-activated calcium channels (HVA) open at higher membrane potentials (16); finally, Ca^{2+}-activated Cl^- channels (CACC) and Ca^{2+}-activated K^+ channels (CAKC) are thought to repolarize the cell (5). Other elements involved in the pathway regulation are the phosphatases and phosphodiesterases, which reduce the cGMP levels (17–19). A schematic representation of the proposed speract-activated signaling pathway in the spermatozoa flagellum of *S. purpuratus* is given in Fig. 1. A complete list of the suggested molecules involved in the signaling pathway is given in Table S1 in the Supporting Material.

Given that various negative interaction loops with three or more nodes can be identified in the above-discussed *S. purpuratus* speract-activated signaling pathway (see Fig. 1), it is compatible with a cyclic $[Ca^{2+}]$ behavior. Nevertheless, we know from the theory of nonlinear dynamics that having the right architecture is a necessary but not sufficient condition for a given dynamic behavior (20).

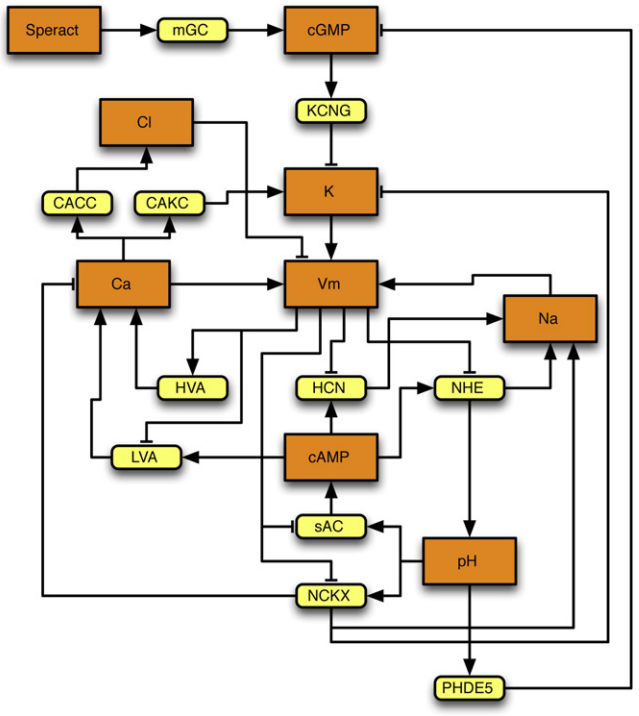

FIGURE 1 Schematic representation of the proposed speract-activated signaling-pathway in the *S. purpuratus* sperm flagellum. (*Large rectangles*) Physiological variables. (*Small round boxes*) Ionic exchangers, ionic channels and enzymes participating in this pathway. For a complete description of the molecules involved, see the main text and Table S1 of the Supporting Material. (*Lines* ending in *arrows*) Positive interactions; (*lines* ending in *hammerheads*) negative interactions.

Therefore, it is important to test whether the suggested architecture for the speract-activated signaling pathway can generate sustained oscillations with a feasible set of parameter values, and if it does, to investigate what the core oscillator is. The work laid out in this article was designed to answer such questions from a mathematical modeling perspective.

MATERIALS AND METHODS

Model development

To keep the model complexity to a minimum, we used a minimalistic strategy to develop a mathematical model for the speract-activated signaling pathway of *S. purpuratus*. With that in mind, we ignored all the steps that set the system ready to cycle but that do not participate in the oscillations themselves. Hence, we disregarded the steps corresponding to the binding of speract to its receptor, the production of cyclic nucleotides, and the increment of intracellular pH. Furthermore, we assumed that the cGMP and cAMP concentrations remain constant during the oscillations, as does the intracellular pH. Finally, we lumped the fluxes associated to the potassium-selective and cyclic nucleotide-gated and low voltage-activated Ca^{2+}-channels with those associated to the CAKC and HVA channels, respectively. The resulting mathematical model consists of five ordinary differential equations, tabulated in Table 1, which describe the dynamics of the Ca^{2+}, Cl^-, Na^+, and K^+ concentrations, as well as the dynamics of the membrane potential (V_m).

The meaning of the symbols in Eqs. 1–5 is as follows: f is the product of Faraday's constant and the flagellum volume, C_m is the flagellar membrane capacitance, I_{Ca} is the HVA current, I_{Cl} is the Ca^{2+}-gated Cl^- current, I_{Na} is the HCN current, I_K is the Ca^{2+}-gated K^+ current, I_{eCa} is the Ca^{2+} current through the NCKX exchanger, I_{eNa} is the Na^+ current through the NCKX exchanger, I_{eK} is the K^+ current through the NCKX exchanger, I_{lCl} is the Cl^- leak current, I_{lNa} is the Na^+ leak current, and I_{lK} is the K^+ leak current.

TABLE 1 Model equations

$$\frac{d[Ca^{2+}]}{dt} = \frac{1}{2f}(I_{Ca} + I_{eCa}). \tag{1}$$

$$\frac{d[Cl^-]}{dt} = -\frac{1}{f}(I_{Cl} + I_{lCl}). \tag{2}$$

$$\frac{d[Na^+]}{dt} = \frac{1}{f}(I_{Na} + I_{eNa} + I_{lNa}). \tag{3}$$

$$\frac{d[K^+]}{dt} = \frac{1}{f}(I_{lK} + I_K + I_{eK}). \tag{4}$$

$$\frac{dVm}{dt} = \frac{1}{C_m}(I_{eCa} + I_{Ca} + I_K + I_{lK} + I_{eK} + I_{Na} + I_{eNa} + I_{lNa} + I_{lCl} + I_{Cl}). \tag{5}$$

The ionic currents in the right-hand side of Eqs. 1–5 are on their own functions of $[Ca^{2+}]$, $[Cl^-]$, $[Na^+]$, $[K^+]$, and V_m. The definitions for each current are given in Table 2.

The meaning of the parameters and variables in Eqs. 6–15 is as follows: E_{Ca}, E_{Cl}, E_{Na}, and E_K represent the Nernst potentials—calculated as $E_i = (RT/zF)\ \ln([ion]_{out}/[ion]_{in})$—for Ca^{2+}, Cl^-, Na^+, and K^+, respectively; g_{Na} is the HCN unitary conductance; g_{Ca} is the HVA unitary conductance; g_K is the CAKC unitary conductance; g_{Cl} is the CACC unitary conductance; N_{Na} is the number of HCN channels; N_{Ca} is the number of HVA channels; N_K is the number of CAKC channels; N_{Cl} is the number of CACC channels; K_{Cl} is the CACC EC_{50} for Ca^{2+}; n_{Cl} is the CACC Hill coefficient for Ca^{2+}; K_K is the CAKC EC_{50} for Ca^{2+}; A_K is the CAKC coefficient of voltage dependence; n_K is the CAKC Hill coefficient for Ca^{2+}; V_{Ca} is the membrane potential needed for half-maximal HVA conductance; K_{Ca} is the HVA coefficient of voltage dependence; V_{Na} is the membrane potential needed for half-maximal HCN conductance; K_{Na} is the HCN coefficient of voltage dependence; e_f is the NCKX exchanger flow rate; l_K is the leakage rate for K^+ influx; l_{Cl} is the leakage rate for Cl^- efflux; and l_{Na} is the leakage rate of efflux of Na^+.

TABLE 2 Ionic currents considered in the model

$$I_{Ca} = \frac{g_{Ca}\, N_{Ca}(E_{Ca} - V_m)}{1 + e^{((V_{Ca} - V_m)/K_{Ca})}}. \tag{6}$$

$$I_{Cl} = \frac{g_{Cl}\, N_{Cl}\, (E_{Cl} - V_m)}{1 + (K_{Cl}/[Ca^{2+}])^{n_{Cl}}}. \tag{7}$$

$$I_{Na} = \frac{g_{Na}\, N_{Na}\, (E_{Na} - V_m)}{1 + e^{((V_{Na} - V_m)/K_{Na})}}. \tag{8}$$

$$I_K = \frac{g_K\, N_K\, (E_K - V_m)}{1 + (K_K/[Ca^{2+}])^{nK} \cdot e^{-V_m/A_K}}. \tag{9}$$

$$I_{eCa} = -2f \cdot e_f \cdot [Ca^{2+}][K^+]. \tag{10}$$

$$I_{eNa} = 4f \cdot e_f \cdot [Ca^{2+}][K^+]. \tag{11}$$

$$I_{eK} = -f \cdot e_f \cdot [Ca^{2+}][K^+]. \tag{12}$$

$$I_{lCl} = f \cdot l_{Cl} \cdot [Cl^-]. \tag{13}$$

$$I_{lNa} = -f \cdot l_{Na} \cdot [Na^+]. \tag{14}$$

$$I_{lK} = f \cdot l_K. \tag{15}$$

It is worth emphasizing that all of the ionic-channel currents are modeled as governed by Ohm's law. Moreover, ion channels can be classified according to their activation mechanism (ligand activation, membrane potential activation, or both). Considering this, we have accounted for each channel activation mechanism in the corresponding conductance term as previously reported (21,22).

The NCKX exchanger uptakes four Na^+ ions, while it expels one Ca^{2+} and one K^+ ion (5). We modeled this exchanger by considering Na^+, Ca^{2+}, and K^+ currents that depend linearly on the Ca^{2+} and K^+ intracellular concentrations.

In the conceptual model described before, the Cl^-, Na^+, and K^+ flows are unidirectional. However, no stationary state would be possible if these were the only flows for such ions. Therefore, we have included in our model linear terms representing leakage currents for these ions.

Parameter estimation

We paid special attention to the estimation of as many parameters as possible from reported experimental data. We were able to estimate in this way 12 of the model's 23 parameters. To estimate the rest of them we varied their values to fit the system dynamic response to reported experimental dynamic results, as discussed in the Results and Discussion. The nominal parameter values employed in this work are given in Table 3, together with the corresponding sources.

Numerical methods

The model set of ordinary differential equations was solved using the algorithm ode23 of MATLAB (The MathWorks, Natick, MA).

RESULTS AND DISCUSSION

We started by numerically solving the model equations, employing the parameter values tabulated in Table 3. Recall that these parameter values correspond to a flagellum stimulated with speract. The results of this simulation are plotted in Fig. 2.

Observe that all the model variables oscillate with a frequency of 2 Hz, in agreement with the reported $[Ca^{2+}]$ oscillation frequency that ranges from 0 to 2 Hz, depending on the speract concentration used to stimulate the sperm (11). Additionally, the $[Ca^{2+}]$ oscillation amplitude predicted by our simulations is similar to that observed experimentally (11). According to our simulations, $[Ca^{2+}]$ oscillations have maximum and minimum values of 1400 nM and 230 nM, respectively, whereas the reported experimental maximum and minimum values for sperms populations are 1200 nM and 300 nM (11).

As discussed before, we were unable to estimate some parameters from reported experimental data, and so we determined their values by fitting the model response to existent dynamic experiments. Hence, the previously reported agreement between our simulations and the experimental results is due in part to such parameter fitting. Nevertheless, it is important to emphasize that the structure of our mathematical model is such that, with a proper choice of parameter values (which are biologically feasible), it can reproduce an oscillatory behavior with the correct amplitude and frequency.

TABLE 3 Model parameters values

Parameter	Description	Units	Value	Reference
f	Product of the Faraday constant and flagellum volume	$C \cdot M^{-1}$	1.54×10^{-10}	FP
C_m	Flagellar membrane capacitance	F	3.14×10^{-13}	FP
g_{Na}	HCN unitary conductance	S	4.3×10^{-11}	(27)
g_{Ca}	HVA unitary conductance	S	7×10^{-12}	(28)
g_K	CAKC unitary conductance	S	4×10^{-12}	FP
g_{Cl}	CACC unitary conductance	S	8×10^{-12}	(29)
N_{Na}	Number of HCN channels		20	FP
N_{Ca}	Number of HVA channels		39	FP
N_K	Number of CAKC channels		80	FP
N_{Cl}	Number of CACC channels		90	FP
K_{Cl}	CACC EC_{50} for Ca^{2+}	M	8.13×10^{-5}	(21)
n_{Cl}	CACC Hill coefficient for Ca^{2+}		1.52	(21)
K_K	CAKC EC_{50} for Ca^{2+}	M	2.83×10^{-10}	(21)
A_K	CAKC coefficient of voltage dependence		1.25×10^{-2}	(21)
n_K	CAKC Hill coefficient for Ca^{2+}		1	(21)
V_{Ca}	Membrane potential needed for half-maximal HVA conductance	V	-1.3×10^{-2}	(30)
K_{Ca}	HVA coefficient of voltage dependence	V	8.8×10^{-3}	(30)
V_{Na}	Membrane potential needed for half-maximal HCN conductance	V	-4.5×10^{-2}	(31)
K_{Na}	HCN coefficient of voltage dependence	V	-1.5×10^{-2}	(31)
e_f	Rate of flow through the NCKX exchanger	$(M \cdot s)^{-1}$	5.45×10^5	FP
l_K	Leakage rate of K^+ influx	$M \cdot s^{-1}$	1.153×10^{-1}	FP
l_{Cl}	Leakage rate of Cl^- efflux	s^{-1}	5.34×10^{-3}	FP
l_{Na}	Leakage rate of Na^+ efflux	s^{-1}	3.9	FP

FP = Fitted parameter.

To further validate our model we simulated two different experiments, reported in Wood et al. (11). In the first one, the authors measured $[Ca^{2+}]$ in a sperm flagellum before speract stimulation. They found that in such a case, the Ca^{2+} concentration reaches a stationary value of 360 nM. To mimic the absence of speract in our model, we reduced the HCN conductance and the NCKX exchanger maximum ionic flux to 95% and 57% of their nominal values, respectively. This is because both HCN channels and NCKX exchangers are stimulated after the addition of speract (5). After numerically solving the model equations, we found that the model variables attain the following steady-state values: 889 nM for $[Ca^{2+}]$, 36.4 mM for $[Cl^-]$, 52 mM for $[Na^+]$, 120 mM for $[K^+]$, and -21.8 mV for V_m. It is important to notice that the only value with an experimental counterpart is $[Ca^{2+}]$, and although the $[Ca^{2+}]$ steady-state value predicted by our model is different from the experimentally reported value, it has the correct order of magnitude.

The second experiment consisted in measuring $[Ca^{2+}]$ over time in a speract-activated sperm treated with niflumic acid. In these sperms, $[Ca^{2+}]$ oscillations were also observed, with amplitude similar to that of the control experiment, but with a reduced frequency (11). It is known that niflumic acid modifies the operation of different types of ionic channels (23). The channels affected in the speract-activated signaling pathway of the *S. purpuratus* sperm are: HCN, CAKC, CACC, and HVA. We found with our model that the reported $[Ca^{2+}]$-oscillation frequency (at ~0.35 Hz) and amplitude (similar to control experiment) can be achieved by, respectively, decreasing the conductance of these channels down to 40%, 34%, 25%, and 90% of their nominal values. The results of the corresponding simulation are plotted in Fig. 3.

Given that we have a reduced number of ion channels participating in the speract-activated signaling pathway, their stochastic gating could have an important effect on the system dynamics. In fact, if the resulting noise is too intense, it could blur the system oscillatory behavior. This question is particularly important because $[Cl^-]$ oscillation amplitude is quite small as compared with the $[Cl^-]$ mean value, as well as with the oscillation amplitude of the other chemical species (see Figs. 2 and 3). To study the system stochastic behavior we assumed that all ion channels randomly switch between the open and closed states.

To calculate the open-state probability distributions, it is useful to recall that the deterministic model is based upon the assumption that the number of open channels of a certain type equals the total channel count, times the probability that each channel is open. Thus, we can calculate the open probability of a given channel as the corresponding current (computed by means of the equations in Table 2), divided by the unitary channel conductance and by the total channel count. Finally, under these assumptions, the number of open channels of each type comes out to be a random variable obeying a binomial distribution, with the open probability computed as discussed above. Note that, as the number of channels tends to infinity, the variation coefficient of the binomial distribution tends to zero, and so the stochastic description turns into a deterministic one.

From the discussion in the previous paragraph, we implemented an Euler-like algorithm to simulate the system

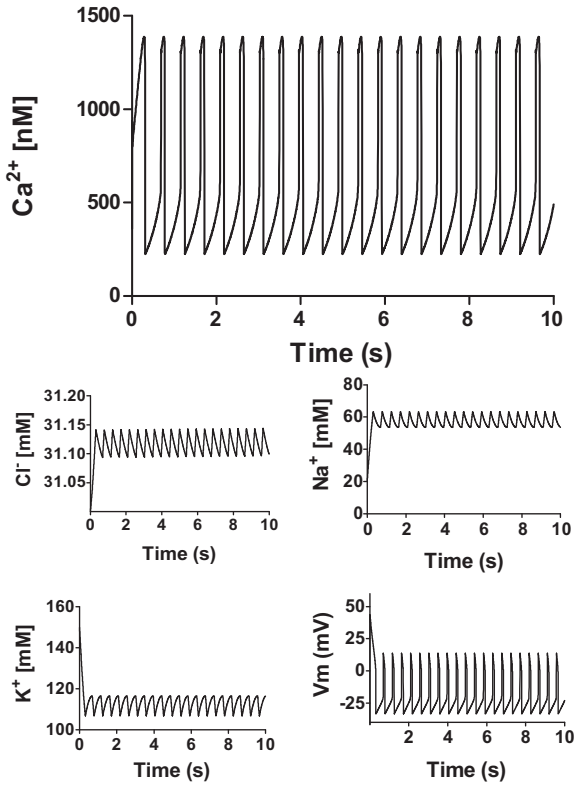

FIGURE 2 Results of a deterministic simulation corresponding to a speract-activated sperm. Each plot represents the dynamics of a model variable versus time (10 s).

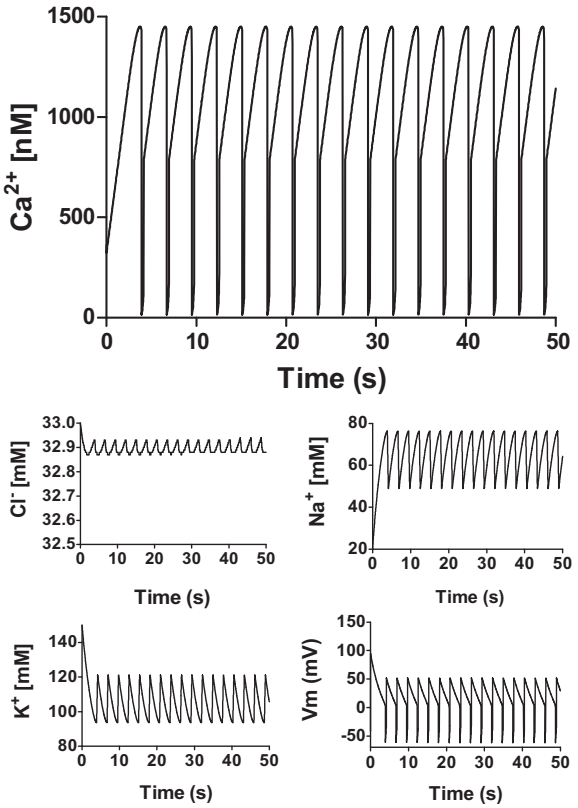

FIGURE 3 Results of a deterministic simulation for a speract-activated sperm treated with niflumic acid. Each plot represents the dynamics of a model variable versus time (50 s).

stochastic behavior as follows. Given the system initial state, we calculated the open probabilities for all the ion channel types, and randomly reckoned the number of open channels by means of the corresponding binomial distributions. Once we knew the open channel counts, we computed the corresponding ionic currents and upgraded the system state accordingly. Finally, the above steps were iteratively repeated until the end of the simulation.

The results of one such stochastic simulation is shown in Fig. 4. To compare with the experiment, the simulated [Ca^{2+}] values were plotted with a sampling period of 0.1 s. Observe that not only is the oscillatory behavior preserved after considering the stochastic gating of all ion channels, but there is a notable resemblance between our model results and those reported in Fig. 2 *B* of Wood et al. (11).

The previously discussed agreement between the model simulations and reported experimental data makes us confident that, despite its simplicity, our model captures the essential details of the real system so as to tackle other questions concerning its dynamic behavior. In particular, we were interested in to find what the core oscillator is, within the speract-activated signaling pathway. Because this question is closely related to the architecture of the interaction network, we computed the Jacobian matrix to study it. We found that the sign of all of the Jacobian entries remains constant for all the values the model variables attain while oscillating. Furthermore, we used the fact that the sign of the Jacobian matrix J_{ij} entry indicates whether the model j^{th} variable affects the i^{th} variable positively (if $J_{ij} > 0$), negatively (if $J_{ij} < 0$), or not at all (if $J_{ij} = 0$), to construct the interaction network depicted in Fig. 5 *A*.

It is known that a negative circuit with at least three nodes can give rise to a limit cycle, in which all the involved variables oscillate (24). We can identify three of this kind of circuit in the network pictured in Fig. 5 *A*: 1), the circuit composed of the *Ca*, *Na*, and V_m nodes; 2), the circuit made up of the nodes *Ca*, *K*, and V_m; and 3), the circuit consisting of nodes *K*, *Na*, and V_m. Hence, the question arises of whether one or more of these circuits is responsible for the system oscillatory behavior. To answer this question we eliminated the nodes *Ca*, *K*, *Na*, and *Cl* (by setting the corresponding variables to their stationary value) one at a time, rendering the networks illustrated in Fig. 5, *B–E*. After numerically solving the equations corresponding to these modified interaction networks (the results are shown in Fig. S1, Fig. S2, Fig. S3, and Fig. S4 of the Supporting Material), we found that only when the subnetwork of nodes *Ca*, *Na*, and V_m is present (Fig. 5, *C* and *E*) does the system show sustained oscillations. Therefore, we conclude that this negative circuit is the core oscillator in this system.

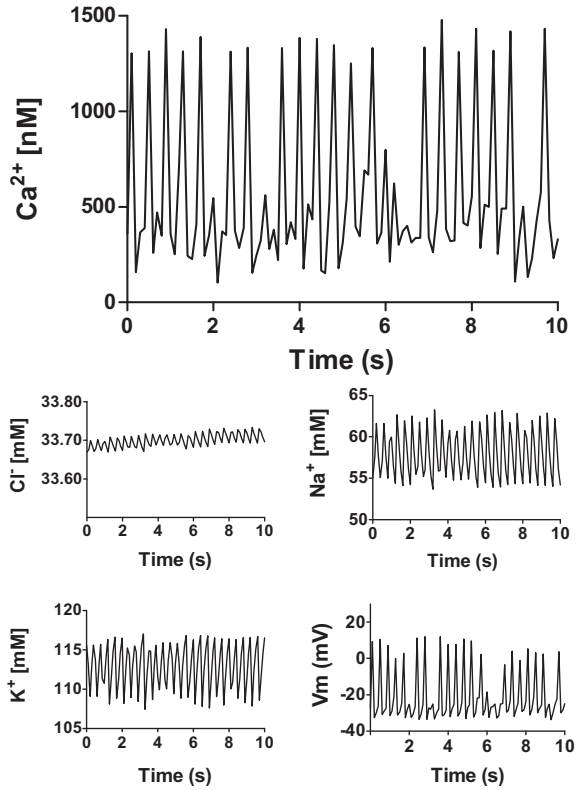

FIGURE 4 Results of a stochastic simulation for a speract-activated sperm. Each plot represents the dynamics of a model variable versus time (10 s).

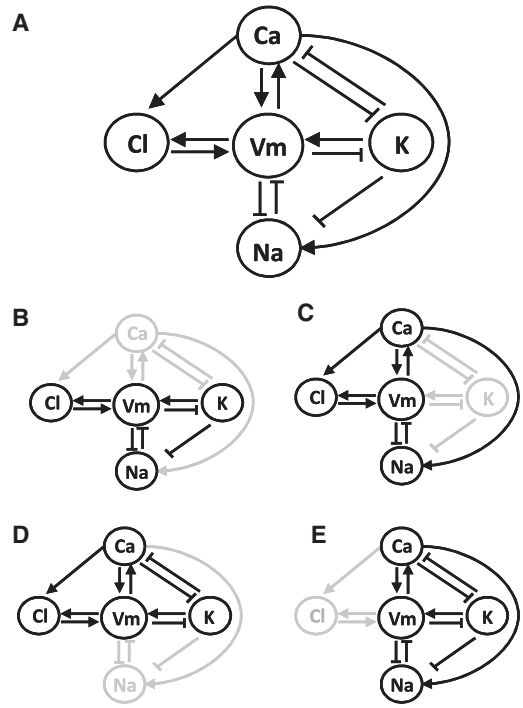

FIGURE 5 Architectures of the system interaction network. (*A*) Complete network. (*B*) Interaction network after elimination of the Ca node. (*C*) Interaction network after elimination of the K node. (*D*) Interaction network after elimination of the Na node. (*E*) Interaction network after elimination of the Cl node. The corresponding simulations are shown in Fig. S1, Fig. S2, Fig. S3, and Fig. S4 of the Supporting Material.

This further implies that the $[K^+]$ and $[Cl^-]$ oscillations occur because the corresponding nodes follow the core oscillator, explaining why the system's inherent stochasticity does not hinder its cyclic behavior, despite the smallness of the $[Cl^-]$ oscillations.

Given that we estimated the values of almost half of the model parameters by fitting according to what will make the model function appropriately, we investigated the robustness of the predicted cyclic behavior to variations on the parameter values. The results are summarized in Table S2 showing the parameter ranges in which an oscillatory behavior is observed, as well as how the oscillation amplitude and frequency change within each parameter range. A general conclusion following from such this table is that the system cyclic behavior is robust to quite-large variations of all the parameter values. Furthermore, we can see there that the oscillation frequency takes values in the range [0 Hz, 3Hz], which compare well with the experimentally observed range of values, [0 Hz, 2Hz] (11).

Of particular interest is the fact that the oscillation frequency increases together with parameters g_{Na} and e_f, which, respectively, stand for the HCN unitary conductance and the rate of flow through the NCKX exchanger. As discussed above, both HCN and NCKX are stimulated after the addition of speract, and the nominal values here employed correspond to a saturating speract dose. We cannot quantitatively study the response of the system to different speract doses, because the corresponding mechanisms are not incorporated into the model. However, the above results allow us to assert that a decreasing speract dose implies smaller g_{Na} and e_f values, and thus a smaller oscillation frequency, in agreement with the experimental observations (11).

CONCLUSIONS

We introduced in this work a mathematical model for the speract-activated signaling pathway in the sperm flagellum of the sea urchin *S. purpuratus*. With such a model we were able to prove that the proposed architecture for this signaling pathway is indeed capable of explaining, with a feasible set of parameter values, an oscillatory behavior with amplitude and frequency similar to those reported (11).

We further tested the model feasibility by simulating two different experiments: a sperm without speract and a speract-activated sperm treated with niflumic acid. In the first case, our model predicted that the system reaches a steady state, with $[Ca^{2+}]$ attaining a stationary value similar to that experimentally reported (11). Moreover, we could reproduce, in the second case, oscillations with frequency and amplitude remarkably similar to those observed in the experiment (11).

We carried out stochastic simulations to investigate the influence of biochemical noise on the system cyclic behavior. Our results demonstrate that the stochastic model still shows sustained oscillations. As a matter of fact, the stochastic simulations reproduce, in a more accurate way, the experimental results for $[Ca^{2+}]$.

A more detailed analysis of the interaction architecture revealed the existence of three subnetworks that could, in principle, be responsible for the system oscillatory behavior. These subnetworks are respectively composed of the nodes *Ca*, *K*, and V_m; *Ca*, *Na*, and V_m; and *K*, *Na*, and V_m. However, we found by sequentially eliminating the *Ca*, *Na*, *K*, and *Cl* nodes that the negative feedback loop consisting of nodes *Ca*, *Na*, and V_m is the system core oscillator. Interestingly, the elimination of the *K* and *Cl* nodes has no apparent effect on the system cycling behavior, even though the Cl^- selective channel has been proposed as a necessary element for the speract-activated signaling pathway to oscillate (9,11).

In contrast with the large amount of experimental evidence, only recently has the speract-activated signaling pathway been studied from a mathematical-modeling perspective (25). Because this study and ours tackle different questions, our results and theirs cannot be directly contrasted in general. Although we are interested in identifying the system core oscillator, Espinal et al. (25) studied, by means of a discrete-dynamics model, the necessary elements for the onset of oscillations. However, among other results, Espinal et al. (25) demonstrated that the CAKC channel plays a central role in determining the period of fluctuations. We simulated the effect of reducing the number of CAKC channels and found that the oscillation period is increased (see Table S2), in agreement with the theoretical and experimental results of Espinal et al. (25). In fact, this last point constitutes one more proof for the validity of our model.

Finally, it is interesting to note that there are different species of sea urchins sharing a common architecture in their SAP-activated pathway. However, only in *A. punctulata* (12) and *Lytechinus pictus* (26) chemotaxis has been experimentally demonstrated. We believe that a mathematical modeling approach would be useful to determine which small differences in the signaling pathways are responsible for this behavior.

SUPPORTING MATERIAL

Two tables, four figures, and references (32–35) are available at http://www.biophysj.org/biophysj/supplemental/S0006-3495(12)00462-6.

This research was partially supported by Consejo Nacional de Ciencia y Tecnología under grants No. 55228 (to M.S.) and No. 82831 (to B.E.G.)

REFERENCES

1. Kaupp, U. B. 2010. Olfactory signaling in vertebrates and insects: differences and commonalities. *Nat. Rev. Neurosci.* 11:188–200.
2. Cukkemane, A., R. Seifert, and U. B. Kaupp. 2011. Cooperative and uncooperative cyclic-nucleotide-gated ion channels. *Trends Biochem. Sci.* 36:55–64.
3. Riffell, J. A., and R. K. Zimmer. 2007. Sex and flow: the consequences of fluid shear for sperm-egg interactions. *J. Exp. Biol.* 210:3644–3660.
4. Publicover, S., C. V. Harper, and C. Barratt. 2007. $[Ca^{2+}]_i$ signaling in sperm—making the most of what you've got. *Nat. Cell Biol.* 9:235–242.
5. Darszon, A., A. Guerrero, …, C. D. Wood. 2008. Sperm-activating peptides in the regulation of ion fluxes, signal transduction and motility. *Int. J. Dev. Biol.* 52:595–606.
6. Kaupp, U. B., N. D. Kashikar, and I. Weyand. 2008. Mechanisms of sperm chemotaxis. *Annu. Rev. Physiol.* 70:93–117.
7. Ward, G. E., C. J. Brokaw, …, V. D. Vacquier. 1985. Chemotaxis of *Arbacia punctulata* spermatozoa to resact, a peptide from the egg jelly layer. *J. Cell Biol.* 101:2324–2329.
8. Brokaw, C. J. 1979. Calcium-induced asymmetrical beating of triton-demembranated sea urchin sperm flagella. *J. Cell Biol.* 82:401–411.
9. Wood, C. D., T. Nishigaki, …, A. Darszon. 2007. Altering the speract-induced ion permeability changes that generate flagellar Ca^{2+} spikes regulates their kinetics and sea urchin sperm motility. *Dev. Biol.* 306:525–537.
10. Wood, C. D., T. Nishigaki, …, A. Darszon. 2005. Real-time analysis of the role of Ca^{2+} in flagellar movement and motility in single sea urchin sperm. *J. Cell Biol.* 169:725–731.
11. Wood, C. D., A. Darszon, and M. Whitaker. 2003. Speract induces calcium oscillations in the sperm tail. *J. Cell Biol.* 161:89–101.
12. Böhmer, M., Q. Van, …, U. B. Kaupp. 2005. Ca^{2+} spikes in the flagellum control chemotactic behavior of sperm. *EMBO J.* 24:2741–2752.
13. Dangott, L. J., J. E. Jordan, …, D. L. Garbers. 1989. Cloning of the mRNA for the protein that crosslinks to the egg peptide speract. *Proc. Natl. Acad. Sci. USA.* 86:2128–2132.
14. Thorpe, D. S., and D. L. Garbers. 1989. The membrane form of guanylate cyclase. Homology with a subunit of the cytoplasmic form of the enzyme. *J. Biol. Chem.* 264:6545–6549.
15. Strünker, T., I. Weyand, …, U. B. Kaupp. 2006. A K^+-selective cGMP-gated ion channel controls chemosensation of sperm. *Nat. Cell Biol.* 8:1149–1154.
16. Granados-Gonzalez, G., I. Mendoza-Lujambio, …, A. Darszon. 2005. Identification of voltage-dependent Ca^{2+} channels in sea urchin sperm. *FEBS Lett.* 579:6667–6672.
17. Ward, G. E., G. W. Moy, and V. D. Vacquier. 1986. Phosphorylation of membrane-bound guanylate cyclase of sea urchin spermatozoa. *J. Cell Biol.* 103:95–101.
18. Ward, G. E., G. W. Moy, and V. D. Vacquier. 1986. Dephosphorylation of sea urchin sperm guanylate cyclase during fertilization. *Adv. Exp. Med. Biol.* 207:359–382.
19. Su, Y. H., and V. D. Vacquier. 2006. Cyclic GMP-specific phosphodiesterase-5 regulates motility of sea urchin spermatozoa. *Mol. Biol. Cell.* 17:114–121.
20. Strogatz, S. H. 1994. Nonlinear Dynamics and Chaos: with Applications in Physics, Biology, Chemistry, and Engineering. Addison-Wesley, Reading, MA, and Wokingham, UK.
21. Gu, Y., P. Lucas, and J. P. Rospars. 2009. Computational model of the insect pheromone transduction cascade. *PLOS Comput. Biol.* 5:e1000321.
22. Dougherty, D. P., G. A. Wright, and A. C. Yew. 2005. Computational model of the cAMP-mediated sensory response and calcium-dependent adaptation in vertebrate olfactory receptor neurons. *Proc. Natl. Acad. Sci. USA.* 102:10415–10420.
23. Cheng, L., and M. C. Sanguinetti. 2009. Niflumic acid alters gating of HCN2 pacemaker channels by interaction with the outer region of S4 voltage sensing domains. *Mol. Pharmacol.* 75:1210–1221.

24. Novák, B., and J. J. Tyson. 2008. Design principles of biochemical oscillators. *Nat. Rev. Mol. Cell Biol.* 9:981–991.

25. Espinal, J., M. Aldana, …, G. Martínez-Mekler. 2011. Discrete dynamics model for the speract-activated Ca^{2+} signaling network relevant to sperm motility. *PLoS ONE.* 6:e22619.

26. Guerrero, A., T. Nishigaki, …, A. Darszon. 2010. Tuning sperm chemotaxis by calcium burst timing. *Dev. Biol.* 344:52–65.

27. Sánchez, D., P. Labarca, and A. Darszon. 2001. Sea urchin sperm cation-selective channels directly modulated by cAMP. *FEBS Lett.* 503:111–115.

28. Hille, B. 1992. Ion Channels of Excitable Membranes, 2nd Ed. Sinauer Associates, Sunderland, MA.

29. Stephan, A. B., E. Y. Shum, …, H. Zhao. 2009. ANO2 is the cilial calcium-activated chloride channel that may mediate olfactory amplification. *Proc. Natl. Acad. Sci. USA.* 106:11776–11781.

30. Sochivko, D., A. Pereverzev, …, H. Beck. 2002. The $Ca_V2.3$ Ca^{2+} channel subunit contributes to R-type Ca^{2+} currents in murine hippocampal and neocortical neurones. *J. Physiol.* 542:699–710.

31. Shin, K. S., C. Maertens, …, G. Yellen. 2004. Inactivation in HCN channels results from reclosure of the activation gate: desensitization to voltage. *Neuron.* 41:737–744.

32. Nomura, M., C. Beltrán, …, V. D. Vacquier. 2005. A soluble adenylyl cyclase from sea urchin spermatozoa. *Gene.* 353:231–238.

33. Galindo, B. E., J. L. de la Vega-Beltrán, …, A. Darszon. 2007. Sp-tetraKCNG: a novel cyclic nucleotide gated K^+ channel. *Biochem. Biophys. Res. Commun.* 354:668–675.

34. Su, Y. H., and V. D. Vacquier. 2002. A flagellar K^+-dependent Na^+/Ca^{2+} exchanger keeps Ca^{2+} low in sea urchin spermatozoa. *Proc. Natl. Acad. Sci. USA.* 99:6743–6748.

35. Gauss, R., R. Seifert, and U. B. Kaupp. 1998. Molecular identification of a hyperpolarization-activated channel in sea urchin sperm. *Nature.* 393:583–587.